AMERICAN SOCIETY FOR MICROBIOLOGY | mBio®

Check for updates

Persister *Escherichia coli* Cells Have a Lower Intracellular pH than Susceptible Cells but Maintain Their pH in Response to Antibiotic Treatment

Olivia Goode,[a,b] Ashley Smith,[a,b] Ashraf Zarkan,[c] Jehangir Cama,[a,d] Brandon M. Invergo,[e] Daaniyah Belgami,[c] Santiago Caño-Muñiz,[c,f] Jeremy Metz,[a,b] Paul O'Neill,[b] Aaron Jeffries,[b] Isobel H. Norville,[g] Jonathan David,[g] David Summers,[c] Stefano Pagliara[a,b]

aLiving Systems Institute, University of Exeter, Exeter, United Kingdom
bSchool of Biosciences, College of Life and Environmental Sciences, University of Exeter, Exeter, United Kingdom
cDepartment of Genetics, University of Cambridge, Cambridge, United Kingdom
dCollege of Engineering, Mathematics and Physical Sciences, University of Exeter, Exeter, United Kingdom
eTranslational Research Exchange at Exeter, University of Exeter, Exeter, United Kingdom
fMRC Laboratory of Molecular Biology, Cambridge, United Kingdom
gDstl, Porton Down, Salisbury, United Kingdom

ABSTRACT Persister and viable but non-culturable (VBNC) cells are two clonal sub-populations that can survive multidrug exposure via a plethora of putative molecular mechanisms. Here, we combine microfluidics, time-lapse microscopy, and a plasmid-encoded fluorescent pH reporter to measure the dynamics of the intracellular pH of individual persister, VBNC, and susceptible *Escherichia coli* cells in response to ampicillin treatment. We found that even before antibiotic exposure, persisters have a lower intracellular pH than those of VBNC and susceptible cells. We then investigated the molecular mechanisms underlying the observed differential pH regulation in persister *E. coli* cells and found that this is linked to the activity of the enzyme tryptophanase, which is encoded by *tnaA*. In fact, in a Δ*tnaA* strain, we found no difference in intracellular pH between persister, VBNC, and susceptible *E. coli* cells. Whole-genome transcriptomic analysis revealed that, besides downregulating tryptophan metabolism, the Δ*tnaA* strain downregulated key pH homeostasis pathways, including the response to pH, oxidation reduction, and several carboxylic acid catabolism processes, compared to levels of expression in the parental strain. Our study sheds light on pH homeostasis, proving that the regulation of intracellular pH is not homogeneous within a clonal population, with a subset of cells displaying a differential pH regulation to perform dedicated functions, including survival after antibiotic treatment.

IMPORTANCE Persister and VBNC cells can phenotypically survive environmental stressors, such as antibiotic treatment, limitation of nutrients, and acid stress, and have been linked to chronic infections and antimicrobial resistance. It has recently been suggested that pH regulation might play a role in an organism's phenotypic survival to antibiotics; however, this hypothesis remains to be tested. Here, we demonstrate that even before antibiotic treatment, cells that will become persisters have a more acidic intracellular pH than clonal cells that will be either susceptible or VBNC upon antibiotic treatment. Moreover, after antibiotic treatment, persisters become more alkaline than VBNC and susceptible *E. coli* cells. This newly found phenotypic feature is remarkable because it distinguishes persister and VBNC cells that have often been thought to display the same dormant phenotype. We then show that this differential pH regulation is abolished in the absence of the enzyme tryptophanase via a major remodeling of bacterial metabolism and pH homeostasis. These new whole-genome transcriptome

data should be taken into account when modeling bacterial metabolism at the crucial transition from exponential to stationary phase. Overall, our findings indicate that the manipulation of the intracellular pH represents a bacterial strategy for surviving antibiotic treatment. In turn, this suggests a strategy for developing persister-targeting antibiotics by interfering with cellular components, such as tryptophanase, that play a major role in pH homeostasis.

KEYWORDS indole, intracellular pH, microfluidics, single-cell analysis, antibiotic resistance, antibiotics, gene sequencing, genomics, persisters, regulation of gene expression, tryptophan operon, viable but non-culturable cells

Fluctuations in environmental conditions can result in phenotypic heterogeneity, for example, in terms of growth rate (1, 2), metabolic activity (3–5), or resistance to stress (6–9), within a clonal population. These cell-to-cell differences allow the population to withstand the challenges posed by dynamic shifts in the environment (10). For example, phenotypic heterogeneity plays an important role in population responses to antibiotic treatment (6, 11). Within an isogenic population, there are at least two phenotypic subpopulations of cells which are able to survive an antibiotic challenge, unlike in the majority of the susceptible population: persister and viable but non-culturable (VBNC) cells (12).

Persisters were first identified by Hobby et al. and Bigger almost 80 years ago, when penicillin was unable to completely sterilize bacterial cultures (13, 14), whereas VBNC cells were identified in 1982 by Xu and coworkers (15). These two subpopulations are able to survive antibiotic exposure. However, whereas persisters are able to resume growth once the antibiotic has been removed, VBNC cells do not resume growth when the antibiotic is removed but might regrow either after a long period of time (from days to months) or when specific conditions, for example, temperature and nutrients, are met (16–19). It is also worth noting that a closely related phenotype, a nongrowing-but-metabolically active state in *Mycobacterium tuberculosis*, is implicated in latent tuberculosis infections and relapses following chemotherapy (20). Two types of persisters have been identified in the literature: triggered and spontaneous, previously called type I and type II, respectively (6, 21). Spontaneous persisters arise during normal growth, unlike triggered persisters, which are generated by stress signals, such as starvation and antibiotic exposure (21). The eventual progenies of both persisters and VBNC cells are as susceptible to antibiotics as the original ancestral culture (14). This feature distinguishes these cells from genetically resistant mutants which possess genetic molecular elements that allow them to survive and replicate during antibiotic treatment (14, 22).

Persister and VBNC subpopulations pose a serious threat to human health and have been associated with chronic infections in immunocompromised patients affected by cystic fibrosis or HIV or those undergoing cancer chemotherapy (12, 23, 24). Persistence has also been linked to the relapse of recurrent diseases, including tuberculosis, candidiasis, salmonellosis, and the diseases caused by *Chlamydia* (25, 26), as well as infections of indwelling devices, such as catheters and heart valves (27). Moreover, there is increasing evidence of a profound link between these antibiotic-surviving phenotypes and the emergence of genetically resistant mutants (28–30).

The exact molecular mechanism for the generation of persister and VBNC cells remains unknown. It has been proposed that stochasticity in the expression of a variety of molecular pathways, such as toxin-antitoxin modules (31–33), the SOS response (34), the alarmone guanosine tetraphosphate (p)ppGpp pathway (33, 35–40), efflux pumps (41), and indole signaling (42–45), may play a role.

Unlike with the previously mentioned pathways, little is known about the role played by intracellular pH heterogeneity within a clonal population with regard to the survival of individual bacteria after an antibiotic challenge (46). The majority of aerobic bacteria, including *Escherichia coli*, are able to grow over a wide range of external pH values, from pH 5.5 to 9 (47, 48). However, excluding extremophiles, most bacteria maintain a near-neutral intracellular pH, this being a vital component of cellular physiology which

bacteria need to tightly control due to the sensitivity of their intracellular enzymatic reactions (47, 49). In addition, metabolic reactions within the cytosol generate protons due to ATP production by glycolysis and oxidative phosphorylation. These processes cause an increase in acidity that the cell counteracts by expelling protons out of the cytosol via proton pumps and remodeling of key metabolic pathways (49–51). This helps maintain a stable electrochemical gradient across the cell membrane, which is vital for respiration (49). The cell regulates intracellular pH not only against internal pH variations but also in response to external stressors. For example, enteric bacteria, such as *E. coli*, must be able to survive in extreme pH ranges, as they need to pass through the stomach to reach a suitable environment for growth and infection (49). Shifting external pH values toward more extreme alkaline or acidic values induces the activation of *rpoS*, the SOS response, and heat shock-like responses, as well as cell-to-cell communication (52–55).

Specifically, cell-to-cell signaling via indole, a ubiquitous signaling molecule produced by over 85 species of bacteria, has recently been linked to the regulation of intracellular pH at the population level (56–58). Indole is synthesized by the enzyme tryptophanase (TnaA), which catalyzes the reversible conversion of tryptophan to indole, ammonia, and pyruvate (59). Indole signaling is involved in a variety of biological processes, such as the regulation of the pathogenicity of cells (60), the tightening of epithelial cell junctions (61), biofilm formation (59, 62), the activation of efflux pumps (44, 45), responses to virulence (44, 63), heat shock (101), and antibiotic stress (64). Two types of indole signaling have been identified: persistent indole signaling, when indole is present at a concentration of around 0.5 mM in the culture medium, and pulse indole signaling, occurring at the transition from the exponential to stationary phases with a maximum intracellular indole concentration of 50 mM, which can be mimicked experimentally by adding 5 mM indole to the culture medium (58). There is an ongoing debate regarding the role played by indole and tryptophan metabolism in antibiotic persistence, with some studies reporting that indole increases the fraction of persisters (65, 66) and others reporting the opposite (42, 43, 67). It is conceivable that these opposing findings might be due to the fact that inhibiting tryptophan metabolism (by genetically knocking out *tnaA* in *E. coli*) might have other profound consequences on bacterial metabolism and pH homeostasis, besides indole production; however, this hypothesis remains to be tested.

In this paper, we set out to quantify the heterogeneity in intracellular pH within a clonal *E. coli* population, aiming to establish whether there is a link between the heterogeneity in intracellular pH and antibiotic survival, which ultimately can dictate the phenotypic structure within a clonal population. Furthermore, we set out to investigate whether the intracellular bacterial pH could be manipulated by interfering with tryptophan metabolism and to determine the genetic and metabolic consequences of the lack of tryptophanase. In order to achieve these aims, we use a microfluidics-microscopy approach (8, 52) in combination with an intracellular pH reporter strain of *E. coli* to investigate the intracellular pH profiles of individual bacteria over time (8, 52). This approach allows us to determine the differences in intracellular pH before, during, and after ampicillin treatment in persister, VBNC, and susceptible bacteria (8, 52). Importantly, we considered bacteria to be VBNC if, after 3 h of antibiotic treatment and 21 h of exposure to antibiotic-free medium, they did not stain with propidium iodide, actively expressed fluorescent proteins, and did not divide within our experimental time frame. This does not exclude the possibility that these cells can start dividing if exposed to nutrients for longer periods of time (19, 68), whereas we can exclude the possibility that these cells are dead (69) since they actively express fluorescent proteins. Next, we used a tryptophanase knockout mutant strain in combination with whole-genome transcriptome analysis and exogenous indole supplementation to investigate the role played by tryptophan metabolism as well as indole signaling on phenotypic survival after exposure to ampicillin and on the maintenance of intracellular pH in the different phenotypic responses to ampicillin. Our data show that cell-to-cell differences in the regulation of intracellular pH represents one of the possible bacterial strategies for escaping antibiotic treatment and therefore might open the way to future therapeutics to

eradicate persister bacteria. Furthermore, this novel approach opens the way for investigating the role of the differential regulation of intracellular pH in individual cells on dynamic responses of microbial populations to external stressors.

RESULTS

E. coli **persisters display a lower intracellular pH than those of VBNC and susceptible cells before ampicillin treatment.** Using time-lapse microscopy, we measured the temporal dynamics of the fluorescence levels of a pH-sensitive green fluorescent protein (GFP) (70, 71), pHluorin, for thousands of individual bacteria as a proxy for intracellular pH (see Materials and Methods). We also measured pHluorin-fused mCherry fluorescence to allow for normalization of any cell-to-cell heterogeneity in protein expression and plasmid copy number. It is worth noting that the fluorescent signals from pHluorin and mCherry were measured in series rather than in parallel by using two different filter sets that allowed for the excitation and the recording of the emission intensity of one of the two fluorophores at a time. This minimizes any artifacts due to potential fluorescence resonance energy transfer between the two fluorophores (72). These microscopy measurements were carried out using a microfluidic mother machine device (73) to image and track each individual bacterium before (time zero [$t = 0$ h]) (Fig. 1a to c) and during ($0 < t < 3$ h) exposure to ampicillin at a concentration of 25× the MIC, as well as during 21 h of exposure to lysogeny broth (LB) ($3 < t < 24$ h) (Fig. 1d to f and Materials and Methods). The mother machine device has previously been employed to investigate bacterial physiology and response to drugs (2, 9, 11, 73–75), and it has been demonstrated that this approach does not introduce cellular stress since both the doubling time and the fraction of persisters measured in the mother machine are in accordance with corresponding measurements performed on cultures growing in flasks or agar plates (9, 73). This single-cell approach allows us to determine the phenotype of each individual bacterium by flowing propidium iodide through the mother machine at 24 h, as previously reported. These phenotypes included persisters (leftmost channel in Fig. 1g), VBNC cells (second channel from the left in Fig. 1g), and susceptible bacteria (two rightmost channels in Fig. 1g) (9). The bacterium in the rightmost channel of Fig. 1g has lysed and disappeared from the channel after ampicillin treatment, whereas the bacterium in the second channel from the right was still visible in the channel but stained with propidium iodide and displayed significantly lower fluorescent protein expression than the VBNC cell; therefore, it was classed as susceptible (Fig. 1f and 1i, Materials and Methods; see also Fig. S1 in the supplemental material) (9). Moreover, the persister progeny were readily killed when exposed to ampicillin a second time at a concentration of 25× MIC at 24 h, confirming that persisters were phenotypically but not genetically resistant to antibiotics.

Crucially, at $t = 0$ h, before ampicillin exposure, VBNC and susceptible *E. coli* subpopulations exhibited a wide range of intracellular pH values, from pH 6.5 to pH 8 (the number of VBNC cells [$n_{\text{VBNC cells}}$] = 104, $n_{\text{susceptible cells}}$ = 2,770; 3 biological replicates), forming a bimodal distribution with peaks around 7.0 and 7.6 (Fig. 2b and c, respectively). In contrast, the persister subpopulation had a tighter regulation of intracellular pH, with a single peak at pH 7.0 ($n_{\text{persister cells}}$ = 30 in 3 biological replicates) (Fig. 2a). This translated into a more acidic intracellular pH in persisters than in VBNC and susceptible bacteria, with mean values of 7.04 ± 0.04, 7.26 ± 0.03, and 7.28 ± 0.01, respectively, before antibiotic treatment. This differential pH regulation between different bacterial phenotypes suggests that the intracellular pH might play a role in survival to drug exposure and thus deserves further investigation.

Abolishing tryptophanase activity eliminates the difference in intracellular pH between persister, VBNC, and susceptible *E. coli* cells before ampicillin treatment. We then tested whether tryptophanase activity and indole production, which have previously been linked to persistence (42, 43, 65–67), play a role in the regulation of intracellular pH in *E. coli* by carrying out the set of experiments described above with a Δ*tnaA* knockout strain (56). In the Δ*tnaA* strain, the initial intracellular pH values of persister, susceptible, and VBNC cells before ampicillin treatment were significantly higher
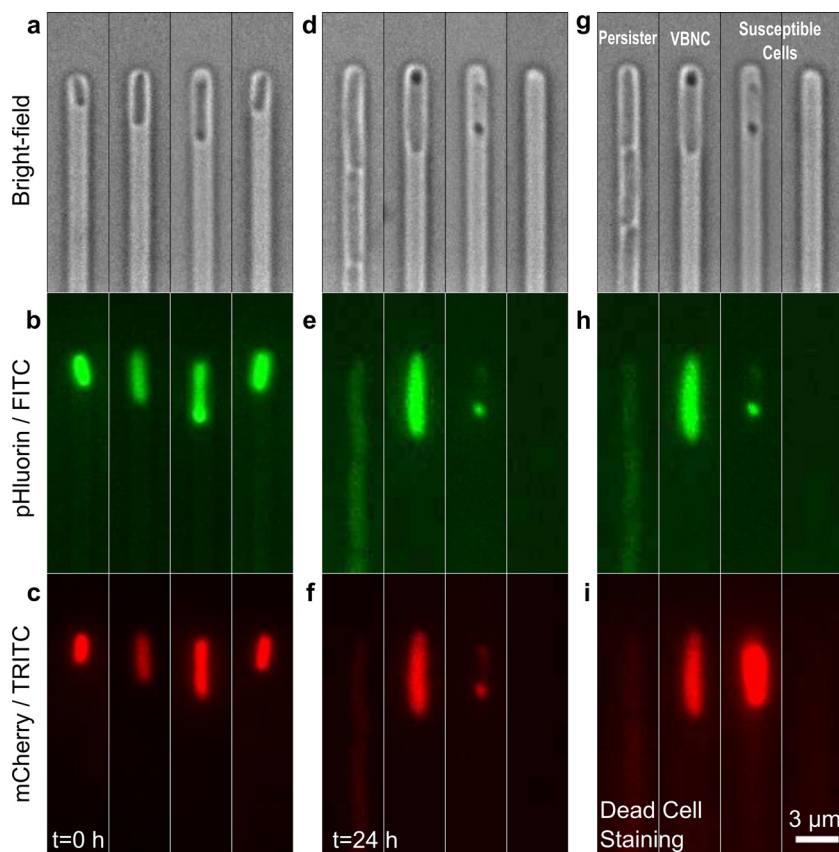
FIG 1 Fluorescence measurement of intracellular pH in individual persister, VBNC, or susceptible *E. coli* cells before and after ampicillin treatment. (a to c) Bright-field, FITC, and TRITC fluorescence images of four representative bacteria injected in the microfluidic mother machine from a 2 μl aliquot that was prepared as follows. A 200 ml 17 h stationary phase *E. coli* BW25113 culture, with a typical OD$_{595}$ of 5, was spun down and resuspended in filtered medium (from the overnight culture) to be adjusted to an OD of 75. 2 μl were withdrawn from this sample and injected into the mother machine. (d to f) Corresponding images of the same bacteria after 3 h of incubation in ampicillin at a concentration of 25× the MIC in an M9-LB (90:10, vol/vol) solution and a successive 21 h of incubation with fresh nutrients. (g to i) Corresponding images of the same bacteria after a 20 min incubation in propidium iodide (PI) to distinguish between susceptible bacteria (second channel from the right), in which PI addition increases the mCherry red fluorescence, and VBNC bacteria (third channel from the right), in which PI addition has no effect on mCherry red fluorescence (Fig. S1). The dynamics of intracellular pH for individual cells in each phenotype was measured by removing the background fluorescence, normalizing the pHluorin against the mCherry signal for each cell at each time point, and using a pH calibration standard (see Materials and Methods). Scale bar, 3 μm.

than the corresponding values measured for the parental *E. coli* strain ($P < 0.0001$), in accordance with previously reported measurements at the population level (56). Crucially, for all three phenotypes of the Δ*tnaA* strain, the intracellular pH distribution displayed a single peak at around 7.5 (Fig. 2e and f); thus, abolishing tryptophanase activity and indole production eliminated the difference in intracellular pH between persister, VBNC, and susceptible cells before antibiotic treatment.

We next set out to determine whether supplementation with indole of a culture of the Δ*tnaA* strain would restore the persister parental-strain phenotype. We chose to perform chemical complementation with exogenous indole, instead of genetic complementation, in order to be able to contrast the effects between the loss of tryptophanase activity and the absence of indole signaling on the regulation of intracellular pH and on the phenotypic composition of the *E. coli* population. We mimicked persistent indole signaling by adding 0.5 mM extracellular indole when inoculating the Δ*tnaA* strain culture in LB or by progressively adding extracellular indole to the growing culture via a syringe pump to recapitulate the indole concentration produced by a
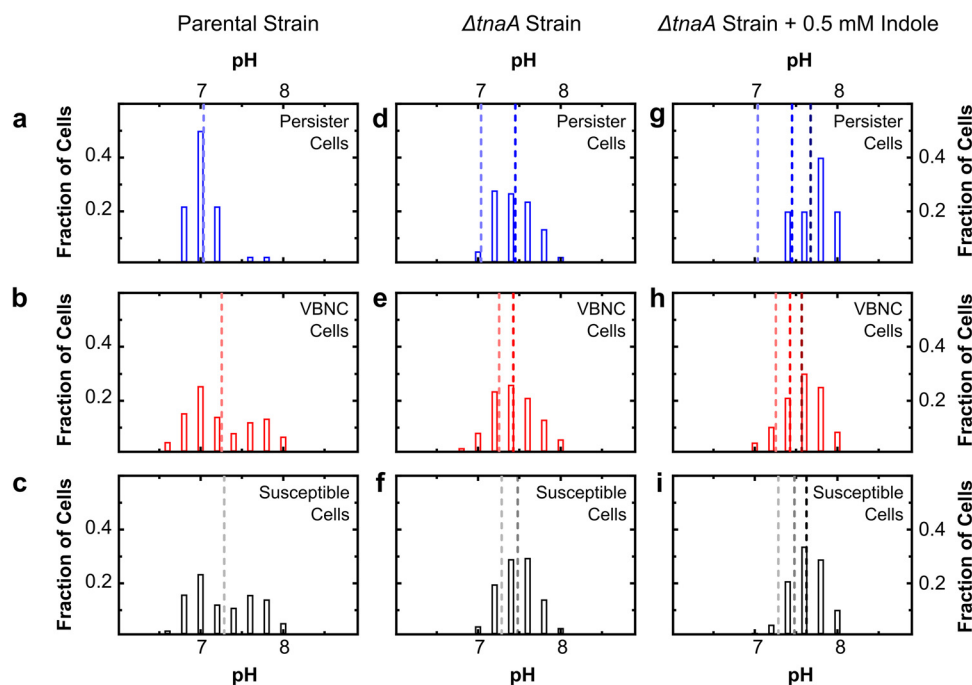
FIG 2 Before ampicillin treatment, persister *E. coli* cells exhibit a more acidic distribution of intracellular pH than susceptible and VBNC *E. coli* cells in an indole-positive strain. (a to c) Distributions of single-cell intracellular pH levels before drug treatment for persister (a), VBNC (b), and susceptible (c) bacteria of the parental *E. coli* strain. (d to f) Corresponding distributions of intracellular pH values for bacteria from the Δ*tnaA E. coli* strain. (g to i) Corresponding distributions of intracellular pH values for bacteria from the Δ*tnaA E. coli* strain with 0.5 mM indole supplementation (see Materials and Methods). Data are collated from at least three biological replicates, with the means of each data set depicted as dashed lines. Each replicate displayed a distribution of intracellular pH values similar to that displayed in the figure. Means of results from panels a to c and d to f are reproduced in panels g to i for comparison purposes only, showing that for all three phenotypes, the parental strain has the most acidic pH and the indole-supplemented Δ*tnaA* mutant has the most alkaline pH. Each strain was cultured at 37 °C for 17 h in LB before injection into a microfluidic device for single-cell pH analysis and subsequent phenotype determination using fluorescence microscopy, as illustrated in Fig. 1 and described in Materials and Methods. For the parental strain, $n_{persister\ cells}$ was 30, $n_{VBNC\ cells}$ was 104, and $n_{susceptible\ cells}$ was 2,770. For the Δ*tnaA* strain, $n_{persister\ cells}$ was 97, $n_{VBNC\ cells}$ was 123, and $n_{susceptible\ cells}$ was 2,907. For the Δ*tnaA* strain with indole, $n_{persister\ cells}$ was 5, $n_{VBNC\ cells}$ was 222, and $n_{susceptible\ cells}$ was 4,729.

growing parental-strain culture (56). We mimicked pulse indole signaling by adding 5 mM extracellular indole for 20 min directly before antibiotic treatment (see Materials and Methods) (56). Pulse indole signaling did not significantly affect the distribution of intracellular pH of the Δ*tnaA* strain, whereas both persistent indole signaling mimics returned similar intracellular pH distributions that were shifted toward alkaline values with respect to the Δ*tnaA* strain (Fig. S2). Therefore, we collated the experimental values gathered by using the former two approaches and found that the initial intracellular pH values of the persister, VBNC, and susceptible cells had alkalinized compared to that of the Δ*tnaA* mutant in the absence of indole (Fig. 2d and g [persister cells], Fig. 2e and h [VBNC cells], and Fig. 2f and i [susceptible cells]).

Taken together, these results suggest that indole supplementation does not restore the intracellular pH profiles observed for persister, VBNC, and susceptible cells in the parental strain. In fact, the addition of indole exacerbates the mean alkalinity of all three phenotypes.

Genetic and metabolic consequences of the absence of tryptophanase. After demonstrating that restoring extracellular indole alone does not restore the intracellular pH regulation observed in the parental strain, we set out to determine which other pathways are affected by the lack of tryptophanase besides the well-known conversion of tryptophan to indole, pyruvate, and ammonia. In order to determine the consequences of the loss of tryptophanase on gene regulation in *E. coli*, we performed genome-wide comparative transcriptome analysis between the parental and the Δ*tnaA* strain by following our previously reported protocols for RNA extraction, sequencing, and
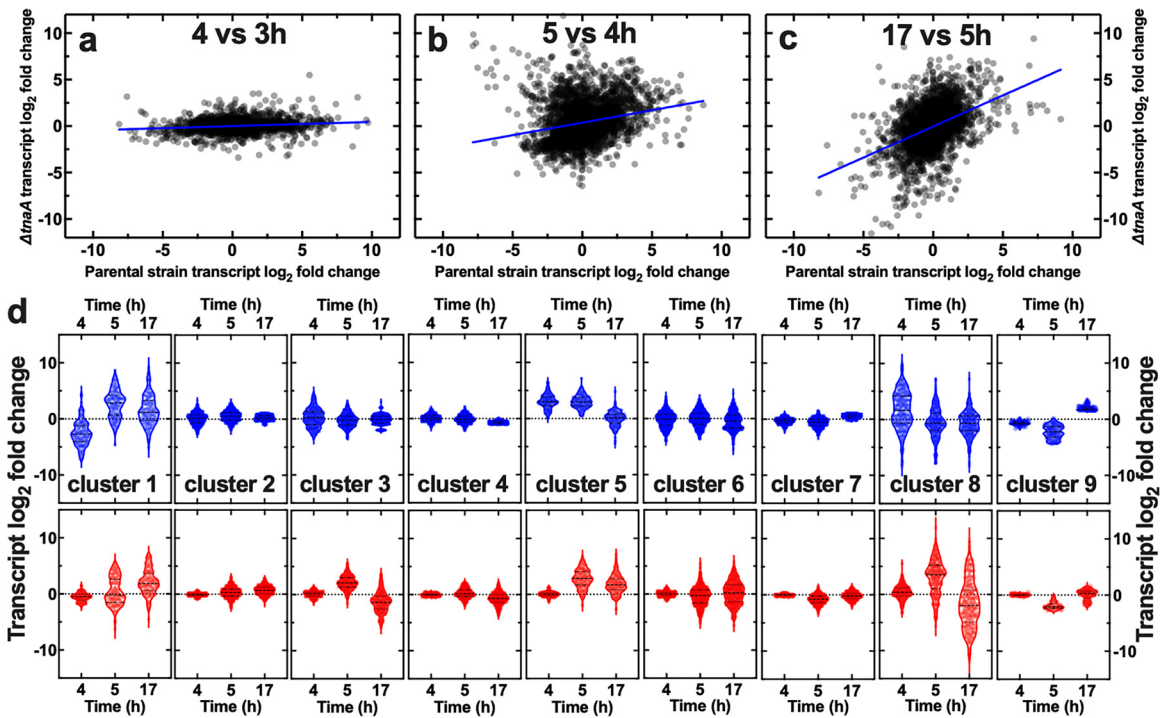
FIG 3 Genetic analysis of the consequences of the lack of tryptophanase. (a to c) Correlations between the $\log_2$ fold changes in transcript reads for the parental and $\Delta tnaA$ strains between 4 and 3 h (a), 5 and 4 h (b), and 17 and 5 h (c). Each dot is the $\log_2$ fold change in transcript reads for a single gene, and blue lines are linear regressions to the data returning Pearson correlation coefficient R values of 0.15, 0.23, and 0.43, respectively. Transcript reads were measured via RNA sequencing of samples in biological triplicates and are reported in Data Set S1. (d) Cluster analysis of the above-described transcriptomic data returned nine clusters with distinct patterns of gene regulation for the parental and $\Delta tnaA$ strains (top and bottom rows, respectively). Each dot represents the $\log_2$ fold change in transcript reads for a single gene, dashed lines indicate the median and quartiles of each distribution, and dotted lines indicate a $\log_2$ fold change of zero. The lists of genes belonging to each cluster are reported in Data Set S1.

analysis from bacterial cultures grown in shaking flasks (see Materials and Methods and reference 76). Considering that *tnaA* expression is strongly upregulated at the transition from exponential to stationary phase (76), we performed RNA sequencing of biological triplicate samples after 3, 4, 5, and 17 h of growth in LB for both the parental and the $\Delta tnaA$ strain. At the whole-genome level, we found a weak correlation between the $\log_2$ fold change in gene expression in the parental and the $\Delta tnaA$ strains between 3 and 4 h (Fig. 3a) ($R = 0.15$), with the mutant displaying a significantly weaker regulation than the parental strain. Remarkably, this is the temporal window when *tnaA* is most strongly upregulated in the parental strain (6.1 $\pm$ 1.1 $\log_2$ fold change) (Data Set S1). In contrast, we found a stronger correlation between the $\log_2$ fold change in gene expression in the parental and the $\Delta tnaA$ strain between 4 and 5 h and between 5 and 17 h (Fig. 3b and c) ($R = 0.23$ and 0.44, respectively) when *tnaA* is downregulated in the parental strain (-0.7 ± 1.1 and -5.6 ± 1.1, respectively). These data suggest a major remodeling of gene regulation in *E. coli* due to the absence of tryptophanase in the 3 to 4 h temporal window, a point on which we expand below.

In order to identify biological processes that were differentially regulated between the $\Delta tnaA$ and the parental strain, we clustered the transcriptomic data above, identifying 9 distinct patterns of gene regulation for the parental and $\Delta tnaA$ strains (top and bottom rows in Fig. 3d, respectively, and Data Set S1). Clusters 5 and 8 most closely resembled *tnaA* regulation in the parental strain (Data Set S1), containing genes with a significantly stronger upregulation at $t = 4$ h in the parental than in the $\Delta tnaA$ strain (3.1 versus 0.1 and 1.7 versus 0.4 mean $\log_2$ fold changes, respectively; $P < 0.0001$ for both) (Fig. 3d). Gene ontology analysis revealed that cluster 8 was enriched for anaerobic respiration, oxidation-reduction, carbohydrate transport, and several catabolic (including *tnaA*) processes (Fig. 4a).

a Biological processes that at t = 4 h are upregulated in the parental compared to the ΔtnaA strain

Cluster 5	Cluster 8
cellular response to stress	anaerobic respiration
response to stress	oxidation-reduction process
response to pH	carbohydrate transport
response to oxygen-containing compound	auxin metabolic process
response to reactive oxygen species	auxin catabolic process
biofilm formation on inanimate substrate	phenylacetate catabolic process
hyperosmotic response	hormone catabolic process
cellular response to reactive oxygen species	small molecule catabolic process
aldehyde catabolic process	toxin catabolic process
cellular response to toxic substance	carboxylic acid catabolic process
response to hydrogen peroxide	toxin metabolic process
glyoxylate metabolic process	xenobiotic catabolic process
cellular response to drug	catabolic process
intraspecies interaction between organisms	organic substance catabolic process
cellular response to oxygen-containing compound	response to xenobiotic stimulus
response to toxic substance	benzene-containing compound metabolic process
cellular response to antibiotic	locomotion
cellular aldehyde metabolic process	response to toxic substance
	cellular catabolic process
	secondary metabolic process
	polyol catabolic process
	cell motility
	localization of cell

b Biological processes that at t = 4 h are downregulated in the parental compared to the ΔtnaA strain

Cluster 1	Cluster 9
iron ion transport	ribonucleoprotein complex biogenesis
iron import into cell	ribosome assembly
cellular transition metal ion homeostasis	ribonucleoprotein complex assembly
transition metal ion homeostasis	ribonucleoprotein complex subunit organization
iron ion homeostasis	organelle organization
siderophore metabolic process	translation
catechol-containing compound metabolic process	peptide metabolic process
secondary metabolite biosynthetic process	RNA processing
establishment of localization in cell	lipopolysaccharide core region biosynthetic process
enterobactin transport	lipopolysaccharide core region metabolic process
nonribosomal peptide biosynthetic process	cellular macromolecule biosynthetic process
secondary metabolic process	macromolecule biosynthetic process
aerobic respiration	gene expression
fatty acid beta-oxidation	cellular protein metabolic process
oxidation-reduction process	oligosaccharide biosynthetic process
organic hydroxy compound biosynthetic process	negative regulation of translation
metallo-sulfur cluster assembly	negative regulation of cellular amide metabolic process
lipid catabolic process	negative regulation of cellular protein metabolic process
cellular lipid catabolic process	methylation
organic hydroxy compound metabolic process	posttranscriptional regulation of gene expression
iron-sulfur cluster assembly	liposaccharide metabolic process
glutamine family amino acid catabolic process	oligosaccharide metabolic process
cellular response to metal ion	polysaccharide metabolic process

FIG 4 Biological processes differentially regulated as a consequence of the lack of tryptophanase. (a) Biological processes significantly overrepresented in gene clusters 5 and 8 (Fig. 3d), which contain genes that at $t=4$ h are upregulated in the parental compared to the ΔtnaA strain. (b) Biological processes significantly overrepresented in gene clusters 1 and 9 (Fig. 3d), containing genes that at $t=4$ h are downregulated in the parental compared to the ΔtnaA strain.

It is worth noting that at the transition from exponential to stationary phase, the environment around *E. coli* BW25113 becomes more acidic, with the extracellular pH reaching a minimum of 6.2 at $t=4$ h, followed by alkalinization of the extracellular environment, with a maximum pH of 7.2 at $t=17$ h (76). Furthermore, cluster 8 was enriched for carboxylic acid catabolic processes (e.g., *tnaA*, *ansB*, *garLR*, *pflB*, and *tdcB*) (Fig. 4a and Data Set S1) that at $t=4$ h are upregulated in the parental but not in the ΔtnaA strain and that further lower the intracellular pH of the parental strain by producing organic acids, such as pyruvic acid (49).

In order to counteract this intracellular acidification, at $t=4$ h, the parental but not the ΔtnaA strain upregulates oxidation-reduction and anaerobic respiration components,

including cytochrome *bd* (*cydAB*), which contributes to the proton motive force, sulfate reductase (*cysH*), and formate (*fdnGHI*), glycerol (*gldA*), sorbitol (*srlD*), and NADH (*wrbA*) dehydrogenases, hydrogenases (*hyaA* and *hybABO*), and other proton-dependent catabolic processes, including lysine (*cadA*) and glutamate (*gadA*) decarboxylases (cluster 8 in Fig. 4a and Data Set S1). Several other proton-independent metabolic pathways are upregulated at $t = 4$ h in the parental but not in the $\Delta tnaA$ strain, including the fumarate (*frdBCD*), dimethyl sulfoxide (*dmsABC*), and nitrate and nitrite (*napA* and *narGHI*, *nirBD*) reductases and the propionate kinase (*tdcD*), as well as anion transport processes, such as alanine (*alaE*) and sulfate (*cysAPU*) transporters (cluster 8 in Data Set S1). Furthermore, gene ontology analysis revealed that cluster 5, which was also upregulated at $t = 4$ h in the parental but not in the $\Delta tnaA$ strain, was enriched in genes for the cellular response to stress, the response to pH, the response to reactive oxygen species, and hyperosmotic response processes (e.g., the aldehyde dehydrogenase *aldB*, the GABA permease *gabP*, the transcriptional regulator *gadX*, the glycine betaine transporter *osmF*, the superoxide dismutase *sodC*, the glutaminase *glsA*, the chaperone *hdeA*, and the deglycases *yhbO* and *hchA*) (cluster 5 in Fig. 4a and Data Set S1). Taken together, these data demonstrate that, thanks to the availability of tryptophanase, the parental strain is capable of performing key metabolic processes that allow the maintenance of a lower intracellular pH than the one displayed by the $\Delta tnaA$ strain, thus providing a mechanistic explanation of our data in Fig. 2 and previous bulk measurements (56).

Clusters 1 and 9 displayed a significantly stronger downregulation at $t = 4$ h in the parental than in the $\Delta tnaA$ strain (-2.6 versus -0.6 and -0.7 versus 0.0 mean $\log_2$ fold changes, respectively; $P < 0.0001$ for both) (Fig. 3d). Cluster 1 was primarily enriched in genes for metal ion transport and homeostasis (e.g., the *fec*, *fep*, and *fhu* operons, *tonB*, and *efeU*), secondary metabolism (e.g., the *ent* operon for the biosynthesis of the siderophore enterobactin), fatty acid metabolism (the fatty acid degradation regulon *fad*), and aerobic respiration (e.g., the cytochrome *bo* genes *cyoABCD*) processes, in contrast with cluster 8, which was enriched in genes for anaerobic respiration (Fig. 4b and Data Set S1). Cluster 9 was primarily enriched in genes for ribonucleoprotein and ribosome assembly (e.g., the 50S ribosomal protein L genes *rplABCDEFKP*), translation (e.g., the 30S ribosomal protein S genes *rpsDEGHKNPQS*), peptide metabolism (e.g., the elongation factor *tufA*), lipopolysaccharide metabolism (e.g., the lipopolysaccharide glucosyltransferase genes *waaBGJPQY*), and macromolecule and oligosaccharide biosynthesis processes (e.g., the transcription elongation factor *greA*) (Fig. 4b and Data Set S1). It is also worth noting that at $t = 4$ h, the $\Delta tnaA$ but not the parental strain upregulated carbohydrate transport processes in order to scavenge for carbon sources in the extracellular environment, especially the fructose-specific phosphotransferase system (*fru* operon) and, to a lesser extent, glucose (*ptsG*) and maltose (*mal* operon) import processes. Taken together, these data suggest that in order to compensate for the decreased availability of intracellular metabolites, such as pyruvate, which is a key intermediate in several metabolic pathways, at $t = 4$ h, the $\Delta tnaA$ strain employed alternative strategies (e.g., iron, carbohydrate, and peptide uptake and metabolism) for maintaining cellular metabolism and cell growth. Finally, clusters 2, 3, 4, 6, and 7 displayed a weak regulation at $t = 4$ h for both the parental and the $\Delta tnaA$ strain (Fig. 5d; Data Set S1), but it is worth noting that the mutant (but not the parental strain) used the cytochrome *bo* (*cyoABCD*) and proton antiporters (*chaA* and *mdfA*) to maintain pH homeostasis in the presence of the acidic extracellular pH.

Overall, this genome-wide transcriptome analysis revealed that abolishing tryptophanase activity causes a major remodeling of the *E. coli* gene expression profile besides abolishing the conversion of tryptophan to pyruvate, indole, and ammonia. Such remodeling includes key processes governing pH homeostasis, thus explaining our findings that the $\Delta tnaA$ strain displays a higher intracellular pH than the parental strain and that indole supplementation alone is not sufficient for lowering the intracellular pH of the mutant.
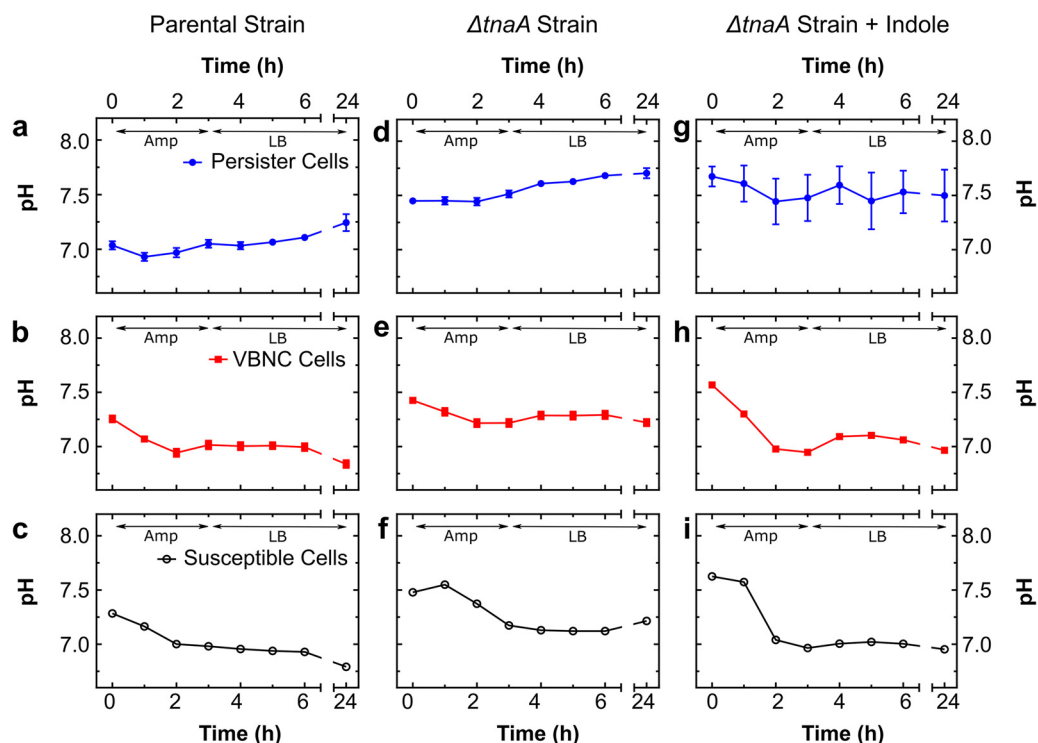
FIG 5 Ampicillin (Amp) treatment acidifies the intracellular pH of VBNC and susceptible bacteria but not of persisters. (a to c) Dynamics of intracellular pH of persister, VBNC, and susceptible *E. coli* cells before drug treatment ($t=0$), during incubation in $25\times$ the MIC of ampicillin in an M9-LB (90:10, vol/vol) solution ($0 < t < 3$ h), and during successive incubation in LB ($3 < t < 24$ h). (d to f) Corresponding dynamics of intracellular pH in a $\Delta tnaA$ *E. coli* strain. (g to i) Corresponding dynamics of intracellular pH in a $\Delta tnaA$ *E. coli* strain with 0.5 mM indole supplementation (see Materials and Methods). The data for each phenotype are presented as means and standard errors of the means from at least three biological replicates. Due to the large sample sizes (reported in Fig. 2), error bars are small compared to the corresponding mean values and are hidden behind some of the data points.

Persister but not VBNC *E. coli* cells are capable of maintaining their intracellular pH during ampicillin treatment. The average intracellular pH of VBNC and susceptible cells in the parental *E. coli* strain decreased as soon as 1 h after ampicillin addition at a concentration of $25\times$ the MIC and reached a minimum of 7.0 after 3 h (Fig. 5b and c). Notably at $t=3$ h, the second peak at pH 7.6 largely disappeared for susceptible and VBNC cells (Fig. S3). After this initial drop in intracellular pH, the VBNC and susceptible cells maintained an average intracellular pH at around 7.0 when incubated in fresh LB at $t=3$ h, reaching a minimum pH of 6.8 at $t=24$ h. In contrast, persisters maintained their intracellular pH during ampicillin treatment and then increased their pH during their successive growth on fresh nutrients, up to a maximum of 7.3 at $t=24$ h (Fig. 5a and Fig. S3). Therefore, after treatment and incubation in LB, the distribution of intracellular pH within the *E. coli* population was completely reversed: persisters that before treatment had the most acidic mean pH were the most alkaline, and conversely, VBNC and susceptible *E. coli* cells that had the most alkaline pH were the most acidic.

Similarly to the parental strain, the $\Delta tnaA$ mutant VBNC and susceptible cells exhibited a drop in intracellular pH after the addition of ampicillin (Fig. 5e and f). Both VBNC and susceptible cells exhibited two further phenotypic responses; a subset of VBNC and susceptible cells maintained a pH at around 7.6 at $t=3$ h, whereas others exhibited a dramatically lower pH, at around 6.8 (Fig. S4). During the successive 21 h of incubation in fresh LB, VBNC and susceptible cells maintained an average intracellular pH of around 7.2 but still displayed two subpopulations at pHs 6.8 and 7.6 at $t=24$ h (Fig. S4). The $\Delta tnaA$ persisters instead increased their pH after ampicillin addition, again as with the parental strain profile, up to a maximum of 7.7 at $t=24$ h (Fig. 5d and Fig. S4).

Finally, when we added 0.5 mM extracellular indole to the $\Delta tnaA$ mutant culture, we found a steep decrease of more than 0.5 in the intracellular pHs of VBNC and susceptible cells after
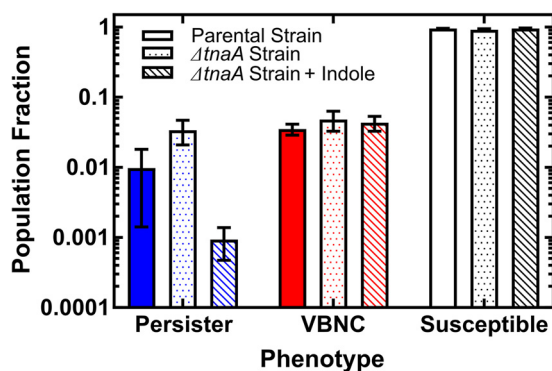
FIG 6 Extracellular indole reduces the fraction of persister but not of VBNC *E. coli* cells. Population fractions for persisters, VBNC cells, and susceptible parental strain *E. coli* cells (blue, red, and black filled bars, respectively) after a 3 h treatment with 25× the MIC of ampicillin. Corresponding population fractions measured for the Δ*tnaA E. coli* strain (dotted bars) and the Δ*tnaA E. coli* strain supplemented with 0.5 mM extracellular indole (hatched bars). Data are presented as means and standard errors of the means from at least 3 biological replicates.

ampicillin addition, down to a minimum of 7 (Fig. 5h and i). In contrast, we did not find a significant change in the intracellular pH of persisters throughout the experiment (Fig. 5g and Fig. S5).

Taken together, these data demonstrate a striking difference between the intracellular pH regulation of persister cells and that of VBNC cells before, during, and after ampicillin treatment, with the VBNC cell intracellular pH profile resembling more closely that of the susceptible cells. Furthermore, these findings suggest that tryptophanase activity and the biological processes associated with it play a role in the regulation of intracellular pH before drug treatment but do not affect the dynamic profile of intracellular pH during antibiotic treatment, which is instead affected by supplementation of extracellular indole.

Abolishing tryptophanase activity increases the fraction of persister but not VBNC *E. coli* cells. Since our microfluidics-microscopy assay allows us to determine the fate of each individual cell after treatment with ampicillin at 25× the MIC, we were able to determine the composition of the microbial population in terms of the abundance of each phenotype in stationary phase, which is the phase investigated in all our single-cell measurements. We found that the fractions of persister, VBNC, and susceptible cells in the parental *E. coli* strain were 0.01, 0.04, and 0.95, respectively (filled bars in Fig. 6), in accordance with previously reported studies (9).

In comparison, the persister fraction of the Δ*tnaA* mutant was over three times higher than that of the parental strain, whereas the fraction of VBNC cells of the Δ*tnaA* mutant was similar to that measured for the parental strain (dotted and filled bars in Fig. 6, respectively). These data are in accordance with persister fractions found in bulk measurements showing that the Δ*tnaA* mutant contains more persisters than the parental strain in stationary phase, which is the growth phase after the indole pulse, which naturally occurs at the transition from exponential to stationary phase (Fig. S6a) (56, 57). In contrast, we found that the opposite occurred in bulk cultures in exponential phase, with a higher fraction of persisters in the parental strain than in the Δ*tnaA* mutant (Fig. S6b).

Next, we set out to determine whether supplementing a stationary phase Δ*tnaA* culture with 0.5 mM indole would restore the persister parental strain phenotype. When we supplemented the Δ*tnaA* mutant culture with indole, we found a decrease in the persister fraction, down to 0.001, which is more than an order of magnitude lower than that measured for the Δ*tnaA* strain in the absence of indole; in contrast, indole addition did not have an impact on the fraction of VBNC cells (Fig. 4). These data suggest that in the absence of tryptophanase, the number of stationary phase *E. coli* cells that are persisters after ampicillin treatment increases; however, chemically restoring persistent indole signaling restores the low persister fraction observed in the parental

strain. Interestingly, we also note that neither tryptophanase activity nor indole signaling affected the composition of the microbial population in terms of the abundance of VBNC cells, which remained unchanged across the different experiments.

DISCUSSION

Maintenance of intracellular pH within a cell is vital for cellular structure, functioning, and pathogenesis (49, 77). pH homeostasis allows correct protein folding, optimum enzymatic activity in metabolic reactions, and growth to take place (78), and it has recently been suggested that it might play a role in phenotypic survival after antibiotic treatments (46); however, this hypothesis remains to be tested. Therefore, we sought to investigate whether cell-to-cell differences in intracellular pH may represent a possible bacterial strategy to evade antibacterial activity.

By measuring the temporal changes in intracellular pH at the single-bacterium level, we found that before antibiotic exposure, *E. coli* persisters that survive ampicillin treatment display a lower intracellular pH than VBNC and susceptible *E. coli* cells. This difference resulted from a tighter regulation of pH in persisters, whereas VBNC and susceptible cells displayed a distribution of pH values, with two local maxima around 7.0 and 7.6. This novel finding represents, to the best of our knowledge, the first evidence of phenotypic differences between persister and VBNC cells before antibiotic treatment. Indeed, due to the difficulty of studying persisters and VBNC cells together, there is minimal literature comparing and contrasting these two phenotypes within the same experiment. The phenotypic differences that we found are notable considering that persister and VBNC cells are often thought to display the same dormant phenotype (26, 79), whereas we demonstrate here that persister and VBNC cells are clearly distinguishable, suggesting that antimicrobials that selectively target persisters could be developed. These data also shed new light on the idea proposed by Bartek et al. that a contributing factor of antibiotic lethality is an antibiotic's effect on bacterial intracellular pH (77). Bartek et al. showed that a number of antibiotics cause an increase in the intracellular pH of *Mycobacterium smegmatis*, thought to disrupt essential processes, with the mechanism remaining unclear. This study also suggested that when a number of pathogens, including *E. coli*, were exposed to conditions which encouraged intracellular acidification, there was a decrease in their susceptibilities to antibiotics, including kanamycin, norfloxacin, and carbenicillin (77). This hypothesis proved to be true in our paper, at least with respect to persister *E. coli* cells displaying a lower pH than the population average before treatment and then surviving supra-MIC ampicillin treatment.

Persisters have been previously linked to indole and tryptophanase activities via a number of processes and stress responses, including multidrug exporters (44), dual-function importers (67), quorum sensing (60), oxidative shock (43, 65), and toxin-antitoxin modules (42). Therefore, we sought to determine the impact of the absence of tryptophanase activity and indole signaling on the intracellular pH values of persister, VBNC, and susceptible cells. Using a ΔtnaA strain, we found that the intracellular pH values of persister, susceptible, and VBNC cells before ampicillin treatment were significantly higher than the corresponding values measured for the parental *E. coli* strain, in accordance with population-level measurements (56). We then demonstrated that providing the ΔtnaA strain with mimics of persistent or pulse indole signaling could not restore the regulation of intracellular pH measured in the parental strain. Taken together, these data suggest that tryptophanase activity is key in maintaining pH homeostasis in response to changes in the pH of the extracellular environment (76) and that processes other than the conversion of tryptophan to indole underlie the observed acidification of stationary phase persisters, compared to VBNC or susceptible cells, preparing them to survive antibiotic challenge and promptly regrow after antibiotic removal.

Neutralophiles, such as *E. coli*, employ two major strategies to maintain pH homeostasis: the regulation of proton transporters, such as pumps and antiporters, and the remodeling of metabolic patterns, chiefly those involved in the production of organic acids (49). Accordingly, our whole-genome transcriptome and cluster analysis revealed

that at the transition from exponential to stationary phase, the Δ*tnaA* strain upregulated a set of transporters that were orthogonal to those in the parental strain. Even more remarkably, the Δ*tnaA* strain significantly remodeled its metabolism compared to that of the parental strain, especially in terms of the use of amino acid decarboxylases, which are known to play a major role in acid resistance (80). Besides the loss of tryptophan conversion to pyruvic acid, which is known to decrease the intracellular pH (82), other key carboxylic acid catabolic processes, as well as oxidation-reduction, response to pH (83), response to reactive oxygen species, and hyperosmotic response components, were upregulated in the parental but not in the Δ*tnaA* strain. In contrast, the Δ*tnaA* but not the parental strain upregulated metal transport, secondary metabolism, fatty acid metabolism, ribosome assembly, translation, and carbohydrate transport processes. It is also worth noting that whereas the parental strain upregulated anaerobic respiration processes in this temporal window, the Δ*tnaA* strain, in contrast, upregulated aerobic respiration processes, and it is known that neutralophiles display different pH responses during anaerobic and aerobic respiration (83).

Overall, this novel knowledge about the genetic and metabolic consequences of the loss of tryptophanase is very important because it explains both our and previous findings that the Δ*tnaA* strain is more alkaline than the parental strain (56) and opens the way for the use of tryptophanase inhibitors (84) to manipulate bacterial metabolism and intracellular pH. Moreover, this novel genome-wide transcriptome analysis constitutes a very valuable resource when modeling bacterial metabolism in response to physicochemical changes in the extracellular environment (85–87), since we show that abolishing tryptophanase activity triggers a major remodeling of bacterial metabolism and pH homeostasis, whereas a previous study showed that indole supplementation alone affects protein expression to a lesser extent (88).

Finally, we sought to investigate the response to antibiotics in terms of both changes in intracellular pH in persister, VBNC, and susceptible cells as well as measuring the relative fractions of these three phenotypes after antibiotic treatment. We found that persisters increased their intracellular pH in the parental and Δ*tnaA* strains with and without indole supplementation, whereas VBNC and susceptible cells became more acidic in response to antibiotic treatment. Therefore, processes that are not linked to indole signaling or tryptophanase activity must underlie the alkalinization of persisters and acidification of VBNC cells in response to ampicillin treatment. It is worth noting that there are conflicting reports on the effect that indole has on the composition of a population in terms of the relative abundances of persister, VBNC, and susceptible cells. Vega et al. (65) and Kuczyńska-Wiśnik et al. (66) found an increase in the abundance of persisters in the presence of indole, whereas Hu et al. (42), Kwan et al. (43), and Wang et al. (67) found the opposite. These inconsistencies are probably due to the different indole concentrations, modes of action of antibiotics applied, types of indole signaling, and phases of cells used between assays (58). Indeed, we also observed a change in persister fraction within our ensemble measurements, depending on certain criteria. In exponential phase, we found a higher proportion of persisters in the parental than in the Δ*tnaA* strain. However, in stationary phase, this phenomenon was reversed, with a higher proportion of persisters found in the Δ*tnaA* than in the parental strain, but mimics of persistent indole signaling restored the persister levels measured for the parental strain. Therefore, the Δ*tnaA* strain appears to be a high-persister-level mutant (21), exhibiting high persister levels in stationary but not in exponential phase, suggesting that persistent indole signaling increases the level of triggered persisters but not of spontaneous persisters (89). Surprisingly, we found that the abundance of VBNC cells within the *E. coli* population was not affected by the removal of either tryptophanase activity or indole signaling. This is important because it contradicts the hypothesis that persister and VBNC cells display the same dormant phenotype (79).

In conclusion, our findings demonstrate that the regulation of intracellular pH is not homogeneous within a clonal population, with persisters displaying differential pH regulation and regrowing after antibiotic treatment. We showed that tryptophanase

activity and several associated metabolic processes that are upregulated at the transition from exponential to stationary phase underpin this differential pH regulation, whereas tryptophanase activity and its associated indole signaling control the fraction of persister cells that survive and regrow after ampicillin treatment. Considering that more than 85 bacterial species encode tryptophanases (90), our data open the way for the manipulation of the intracellular pH and phenotypic compositions of microbial populations by developing and using tryptophanase-targeting compounds.

MATERIALS AND METHODS

Strains and culture conditions. All chemicals were purchased from Fisher Scientific or Sigma-Aldrich unless otherwise stated. Cells were cultured using LB medium (10 g/liter tryptone, 5 g/liter yeast extract, and 10 g/liter NaCl; Melford) and LB agar plates (15 g/liter agar). Minimal medium (M9) was made from $1\times$ M9 salts, 2 mM $MgSO_4$, and 0.1 mM $CaCl_2$ in deionized water. The medium was autoclaved before the addition of sterile thiamine hydrochloride, for a final concentration of 3 μM. E. coli BW25113 parental and $\Delta tnaA$ strains were obtained from the Keio collection (91, 92). Both strains were transformed with the pSCM002 plasmid, which expresses the mCherry-pHluorin translational fusion protein under an arabinose-inducible promoter and carries a chloramphenicol resistance marker. pSCM002 was constructed from pSCM001 (Addgene; 124605) (56) by swapping the ampicillin resistance marker with a chloramphenicol resistance marker. Briefly, PCR was used to amplify two fragments: a chloramphenicol resistance marker from pT2SC (Addgene 59382) and pSCM001, excluding the ampicillin resistance marker (93). Each fragment was amplified with flanking regions homologous to the other fragment. The two fragments were ligated using a Gibson assembly kit (NEB) (94) to generate a pBAD TOPO plasmid containing an mCherry-pHluorin translational fusion and a chloramphenicol resistance marker, pSCM002. The sequences of primers used to generate the pSCM002 plasmid are available in the supplemental material (Table S1). pHluorin (supercliptic pHluorin) is a green fluorescent reporter for intracellular pH derived from GFP with 8 amino acid changes (F64L, S65T, S147D, N149Q, T161I, S202F, Q204T, and A206T) (70, 71). mCherry fluorescence is not affected by pH and was therefore used to normalize changes in fluorescence caused by cell-to-cell variation in protein expression and differences in plasmid copy numbers between the exponential and stationary phases. Cultures were streaked on LB agar supplemented with chloramphenicol (25 μg/ml) for plasmid maintenance and incubated overnight at 37 °C to obtain single colonies. Overnight liquid cultures were prepared with a single colony from a streak plate and grown in 200 ml of LB medium supplemented with chloramphenicol (25 μg/ml) and arabinose (5 μg/ml) for 17 h at 37 °C on a shaking incubator at 200 rpm. When required, 0.5 mM indole (dissolved in absolute ethanol) was supplemented at the beginning of an overnight culture of the $\Delta tnaA$ strain.

Microfluidic device fabrication. The mother machine microfluidic device was fabricated by pouring a 9:1 (base-to-curing agent) polydimethylsiloxane (PDMS) mixture into an epoxy mold kindly provided by S. Jun, as previously described (95). The PDMS was cured at 70 °C for 2 h and then peeled from the epoxy mold to obtain 12 individual chips. Fluidic access was achieved using a 0.75 mm biopsy punch (Harris Uni-Core; WPI). The microfluidic device was assembled by bonding the PDMS chip to a glass coverslip, both of which were exposed to an air plasma treatment for 10 s at a 30 W plasma power (plasma etcher; Diener, Royal Oak, MI, USA) and then placed in contact to irreversibly bond the PDMS chip to the glass coverslip. The plasma treatment temporarily renders the device hydrophilic, so within 5 min post-bonding, the device was filled with 2 μl of 50 mg/ml bovine serum albumin (BSA) solution and incubated at 37 °C for an hour to prevent cell adhesion to the internal surfaces of the device.

Microfluidics-microscopy assay to measure intracellular pH in individual cells. An overnight culture was prepared by incubating E. coli in LB at 37 °C for 17 h with agitation at 200 rpm. Bacteria were harvested from the overnight culture via centrifugation for 10 min at 4,000 rpm at room temperature (Eppendorf 5810 R). The supernatant was filtered twice (medical Millex-GS filter, 0.22 μm; Millipore Corp.) and used to resuspend the bacteria to an optical density at 595 nm (OD_{595}) of 75; additionally, BSA was added to the bacterial suspension at a concentration of 0.5 mg/ml. Two microliters of the bacterial suspension was injected into the microfluidic device and incubated at 37 °C until there were 1 to 2 bacteria in the lateral side channels. Fluorinated ethylene propylene tubing (1/32 in. by 0.008 in.) was connected to the inlet and outlet holes and connected to a flow rate measuring device (Flow Unit S; Fluigent, Paris, France) and outlet reservoir, respectively. The flow rate measuring device was regulated by a computerized pressure-based flow control system (MFCS-4C; Fluigent) controlled by MAESFLO software (Fluigent). Spent medium was flushed through the device to wash excess bacteria out of the main channel at 300 μl/h for 8 min to completely exchange the fluid in the device and tubing. The chip was mounted on an inverted microscope (IX73 Olympus, Tokyo, Japan), and images were acquired in bright-field and two fluorescence modes. Images were collected via a 60$\times$, 1.2 numerical aperture (NA) objective (UPLSAPO60XW; Olympus) and an sCMOS camera (Zyla 4.2; Andor, Belfast, UK). The fluorescence modes used a fluorescein isothiocyanate (FITC) and tetramethyl rhodamine isothiocyanate (TRITC) filter, exposing the bacteria to blue and green excitation bands of broad-spectrum LEDs at 20% and 5% of their intensity, respectively, for 0.03 s. The microfluidic device was moved by two automated stages (M-545.USC and P-545.3C7 [Physik Instrumente, Karlsruhe, Germany] for coarse and fine movements, respectively) to image multiple fields of view in a sequential manner. The imaging setup was controlled by LabView, with automated shutter and filter switching. After acquiring the first set of images, we allowed 25$\times$ the MIC of ampicillin to flow in a 90:10, vol/vol, M9-LB solution at 300 μl/h for 8 min before lowering the flow rate to 100 μl/h for 3 h. After

3 h of treatment, LB medium was flushed through the chip at 300 μl/h for 8 min before the rate was lowered to 50 μl/h for 21 h. Images were taken hourly between $t = 0$ and $t = 6$ h and at 24 h. At 24 h, propidium iodide (PI) was used to flow through the microfluidic device for 15 min according to the manufacturer's specifications. Bright-field and fluorescence images were acquired to distinguish between VBNC and SNL cells using 5% green LED intensity with a TRITC filter for 0.03 s. All experiments were carried out at room temperature.

Indole supplementation. Three indole supplementation protocols were tested to recover the parental strain in the Δ*tnaA* strain. The first protocol used addition of indole to a final concentration of 0.5 mM at the start of a culture and then incubation overnight as previously described. The second protocol mimicked the previously specified indole pulse (56, 57) by supplementing indole at a final concentration of 5 mM for 20 min once the 17 h overnight Δ*tnaA* culture was loaded in the microfluidic device. The third protocol used a portable syringe pump (Chemyx Inc.) to dynamically drip indole into a growing Δ*tnaA* culture for 200 min to mimic the external indole concentration previously recorded by Zarkan et al. (56). The results from all three indole supplementation methodologies are reported in Fig. S2.

Intracellular pH determination via single-cell fluorescence. pHluorin fluorescence intensity has a linear relationship with pH between pH 6.5 and pH 8 (71). The fluorescence intensity of mCherry is unaffected by pH and was used to normalize the pHluorin fluorescence due to variations in protein expression and plasmid copy number between individual cells. To equate the relative fluorescence of each cell to a pH value, the intensity ratio of pHluorin to mCherry for each cell was calculated and, with a calibration curve, converted to a pH value. The standard curve was generated by exposing the parental strain and Δ*tnaA* mutant to 50 μM carbonyl cyanide *m*-chlorophenyl hydrazine (CCCP) at 300 μl/h for 8 min and then at 100 μl/h for 20 min, which causes the intracellular pH to equalize to the pH of the medium by allowing the translocation of protons across the cytoplasmic membrane (56). PBS solutions whose pHs were manually adjusted to 6.5, 7.0, 7.5, and 8.0 were used to generate the standard curve using the same imaging/experimental settings described above. The relationship between fluorescence and pH obtained from the standard curve was used to calibrate all pH values in our experiments.

Image and data analysis. All image analysis was performed using a custom Python module, MMHelper (96). In brief, channels and bacteria were detected by using automated thresholding algorithms and were assigned unique numeric labels. Each bacterium in a frame was tracked, and a lineage was established and then manually verified. Note the increase in red fluorescence of the susceptible but not of the VBNC cells, thus indicating the susceptibility of the cell. By normalizing the pH-sensitive pHluorin intensity against the mCherry intensity, which is unaffected by pH, for each bacterium at each time point, we accounted for variation in protein expression and plasmid copy number between individual cells. We determined the intracellular pH of individual cells from their relative fluorescence by using a calibration curve.

For each lineage, the corresponding masks were used to extract the width, length, area, and fluorescence intensities of the individual bacteria from the corresponding fluorescence images. The background fluorescence was established from the average fluorescence for the areas of the channels that did not contain bacteria and subtracted from the fluorescence intensity measured on each bacterium. The information for all bacteria within a frame across the different time points was written into .csv files. Each bacterium was labeled manually as a persister, a VBNC cell, a susceptible lysed cell, or a susceptible nonlysed cell. The data presented in this paper were plotted using GraphPad Prism 8 and represent means and standard errors of the means from at least 3 biological replicates. Due to the large sample sizes, error bars are small compared to the corresponding mean values and are hidden behind the data points in some of the graphs. Statistical significance was tested by an unpaired *t* test with Welch's correction.

Transcriptomic analysis. RNA isolation, library preparation, sequencing, and transcriptomic data processing were performed as previously reported (76). Briefly, parental and Δ*tnaA E. coli* cultures were prepared as described above, and 500 μl aliquots were taken after $t = 3$, 4, 5, and 17 h after inoculation in LB in biological triplicates. RNAprotect bacterial reagent (Qiagen) was added to each aliquot. Extractions were performed using an RNeasy minikit (Qiagen) by following the manufacturer's instructions. DNA removal during extraction was carried out by using RNase-Free DNase I (Qiagen). RNA concentration and quality were measured using a Qubit 1.0 fluorometer (ThermoFisher Scientific) and 2200 TapeStation (Agilent), respectively, and only samples with an RNA integrity number larger than 8 were taken forward. Transcript abundance was quantified using Salmon for each gene in all samples. Subsequent differential analysis was performed using DEseq2 in R software to quantify the log$_2$ fold change in transcript reads (97) for each gene.

Cluster and gene ontology analysis. Clustering analysis of the transcriptome data was performed using the mclust 5 package (version 5.4.7) for R (98). Using this method, a Gaussian finite mixture model was estimated for all transcript log$_2$ fold change data, with 6 total dimensions (3 time point comparisons across 2 genotypes). The method was configured to test all possible models (e.g., hyperspherical versus ellipsoidal cluster shapes, equal volume versus various volume clusters, etc.), for a range of 2 to 20 total clusters. The minimal, best-fitting model was identified by the Bayes information criterion as 9 ellipsoidal clusters with equal shapes and orientations. Gene Ontology enrichment analysis was performed using the clusterProfiler package (version 3.16.1) for R (99). Enrichment in terms belonging to the "Biological Process" ontology was calculated for each gene cluster, relative to the set of all genes quantified in the experiment, via a one-sided Fisher exact test (hypergeometric test). *P* values were adjusted for false discovery by using the method of Benjamini and Hochberg (100). Finally, the lists of significantly enriched terms were simplified to remove redundant terms, as assessed via their semantic similarity to other enriched terms, using clusterProfiler's simplify function.

SUPPLEMENTAL MATERIAL

Supplemental material is available online only.

FIG S1, DOCX file, 0.1 MB.

FIG S2, DOCX file, 0.1 MB.

FIG S3, DOCX file, 0.1 MB.

FIG S4, DOCX file, 0.1 MB.

FIG S5, DOCX file, 0.1 MB.

FIG S6, DOCX file, 0.1 MB.

TABLE S1, DOCX file, 0.01 MB.

DATA SET S1, XLSX file, 1.1 MB.

ACKNOWLEDGMENTS

REFERENCES

1. Kotte O, Volkmer B, Radzikowski JL, Heinemann M. 2014. Phenotypic bistability in Escherichia coli's central carbon metabolism. Mol Syst Biol 10:736–736. https://doi.org/10.15252/msb.20135022.

2. Łapińska U, Glover G, Capilla-Lasheras P, Young AJ, Pagliara S. 2019. Bacterial ageing in the absence of external stressors. Philos Trans R Soc Lond B Biol Sci 374:20180442. https://doi.org/10.1098/rstb.2018.0442.

3. Şimşek E, Kim M. 2018. The emergence of metabolic heterogeneity and diverse growth responses in isogenic bacterial cells. ISME J 12:1199–1209. https://doi.org/10.1038/s41396-017-0036-2.

4. Nikolic N, Barner T, Ackermann M. 2013. Analysis of fluorescent reporters indicates heterogeneity in glucose uptake and utilization in clonal bacterial populations. BMC Microbiol 13:258. https://doi.org/10.1186/1471-2180-13-258.

5. Kiviet DJ, Nghe P, Walker N, Boulineau S, Sunderlikova V, Tans SJ. 2014. Stochasticity of metabolism and growth at the single-cell level. Nature 514:376–379. https://doi.org/10.1038/nature13582.

6. Balaban NQ, Merrin J, Chait R, Kowalik L, Leibler S. 2004. Bacterial persistence as a phenotypic switch. Science 305:1622–1625. https://doi.org/10.1126/science.1099390.

7. Levy SF, Ziv N, Siegal ML. 2012. Bet hedging in yeast by heterogeneous, age-correlated expression of a stress protectant. PLoS Biol 10:e1001325. https://doi.org/10.1371/journal.pbio.1001325.

8. Wakamoto Y, Dhar N, Chait R, Schneider K, Signorino-Gelo F, Leibler S, McKinney JD. 2013. Dynamic persistence of antibiotic-stressed mycobacteria. Science 339:91–95. https://doi.org/10.1126/science.1229858.

9. Bamford RA, Smith A, Metz J, Glover G, Titball RW, Pagliara S. 2017. Investigating the physiology of viable but non-culturable bacteria by microfluidics and time-lapse microscopy. BMC Biol 15:121. https://doi.org/10.1186/s12915-017-0465-4.

10. Richards TA, Massana R, Pagliara S, Hall N. 2019. Single cell ecology. Philos Trans R Soc Lond B Biol Sci 374:20190076. https://doi.org/10.1098/rstb.2019.0076.

11. Bergmiller T, Andersson AMC, Tomasek K, Balleza E, Kiviet DJ, Hauschild R, Tkačik G, Guet CC. 2017. Biased partitioning of the multidrug efflux pump AcrAB-TolC underlies long-lived phenotypic heterogeneity. Science 356:311–315. https://doi.org/10.1126/science.aaf4762.

12. Lewis K. 2010. Persister cells. Annu Rev Microbiol 64:357–372. https://doi.org/10.1146/annurev.micro.112408.134306.

13. Hobby GL, Meyer K, Chaffee E. 1942. Observations on the mechanism of action of penicillin. Proc Soc Exp Biol Med 50:281–285. https://doi.org/10.3181/00379727-50-13773.

14. Bigger J. 1944. Treatment of staphylococcal infections with penicillin by intermittent sterilisation. Lancet 244:497–500. https://doi.org/10.1016/S0140-6736(00)74210-3.

15. Xu H-S, Roberts N, Singleton FL, Attwell RW, Grimes DJ, Colwell RR. 1982. Survival and viability of nonculturable Escherichia coli and Vibrio cholerae in the estuarine and marine environment. Microb Ecol 8:313–323. https://doi.org/10.1007/BF02010671.

16. Li L, Mendis N, Trigui H, Oliver JD, Faucher SP. 2014. The importance of the viable but non-culturable state in human bacterial pathogens. Front Microbiol 5:258.

17. Pinto D, Almeida V, Almeida Santos M, Chambel L. 2011. Resuscitation of Escherichia coli VBNC cells depends on a variety of environmental or chemical stimuli. J Appl Microbiol 110:1601–1611. https://doi.org/10.1111/j.1365-2672.2011.05016.x.

18. Baffone W, Citterio B, Vittoria E, Casaroli A, Campana R, Falzano L, Donelli G. 2003. Retention of virulence in viable but non-culturable halophilic Vibrio spp. Int J Food Microbiol 89:31–39. https://doi.org/10.1016/S0168-1605(03)00102-8.

19. Wagley S, Morcrette H, Kovacs-Simon A, Yang ZR, Power A, Tennant RK, Love J, Murray N, Titball RW, Butler CS. 2021. Bacterial dormancy: a subpopulation of viable but non-culturable cells demonstrates better fitness for revival. PLoS Pathog 17:e1009194. https://doi.org/10.1371/journal.ppat.1009194.

20. Manina G, Dhar N, McKinney JD. 2015. Stress and host immunity amplify mycobacterium tuberculosis phenotypic heterogeneity and induce nongrowing metabolically active forms. Cell Host Microbe 17:32–46. https://doi.org/10.1016/j.chom.2014.11.016.

21. Balaban NQ, Helaine S, Lewis K, Ackermann M, Aldridge B, Andersson DI, Brynildsen MP, Bumann D, Camilli A, Collins JJ, Dehio C, Fortune S, Ghigo J-M, Hardt W-D, Harms A, Heinemann M, Hung DT, Jenal U, Levin BR, Michiels J, Storz G, Tan M-W, Tenson T, Van Melderen L, Zinkernagel A. 2019. Definitions and guidelines for research on antibiotic persistence. Nat Rev Microbiol 17:441–448. https://doi.org/10.1038/s41579-019-0196-3.

22. Keren I, Kaldalu N, Spoering A, Wang Y, Lewis K. 2004. Persister cells and tolerance to antimicrobials. FEMS Microbiol Lett 230:13–18. https://doi.org/10.1016/S0378-1097(03)00856-5.

23. Brooun A, Liu S, Lewis K. 2000. A dose-response study of antibiotic resistance in Pseudomonas aeruginosa biofilms. Antimicrob Agents Chemother 44:640–646. https://doi.org/10.1128/AAC.44.3.640-646.2000.

24. Spoering AL, Lewis K. 2001. Biofilms and planktonic cells of Pseudomonas aeruginosa have similar resistance to killing by antimicrobials. J Bacteriol 183:6746–6751. https://doi.org/10.1128/JB.183.23.6746-6751.2001.

25. Fauvart M, de Groote VN, Michiels J. 2011. Role of persister cells in chronic infections: clinical relevance and perspectives on anti-persister therapies. J Med Microbiol 60:699–709. https://doi.org/10.1099/jmm.0.030932-0.

26. Ayrapetyan M, Williams TC, Oliver JD. 2015. Bridging the gap between viable but non-culturable and antibiotic persistent bacteria. Trends Microbiol 23:7–13. https://doi.org/10.1016/j.tim.2014.09.004.

27. Lewis K. 2007. Persister cells, dormancy and infectious disease. Nat Rev Microbiol 5:48–56. https://doi.org/10.1038/nrmicro1557.

28. Windels EM, Michiels JE, Van Den Bergh B, Fauvart M, Michiels J. 2019. Antibiotics: combatting tolerance to stop resistance. mBio 10:e02095-19. https://doi.org/10.1128/mBio.02095-19.

29. Levin-Reisman I, Ronin I, Gefen O, Braniss I, Shoresh N, Balaban NQ. 2017. Antibiotic tolerance facilitates the evolution of resistance. Science 355:826–830. https://doi.org/10.1126/science.aaj2191.

30. Levin-Reisman I, Brauner A, Ronin I, Balaban NQ. 2019. Epistasis between antibiotic tolerance, persistence, and resistance mutations. Proc Natl Acad Sci U S A 116:14734–14739. https://doi.org/10.1073/pnas.1906169116.

31. Moyed HS, Bertrand KP. 1983. hipA, a newly recognized gene of Escherichia coli K-12 that affects frequency of persistence after inhibition of murein synthesis. J Bacteriol 155:768–775. https://doi.org/10.1128/jb.155.2.768-775.1983.

32. Vázquez-Laslop N, Lee H, Neyfakh AA. 2006. Increased persistence in Escherichia coli caused by controlled expression of toxins or other unrelated proteins. J Bacteriol 188:3494–3497. https://doi.org/10.1128/JB.188.10.3494-3497.2006.

33. Keren I, Shah D, Spoering A, Kaldalu N, Lewis K. 2004. Specialized persister cells and the mechanism of multidrug tolerance in Escherichia coli. J Bacteriol 186:8172–8180. https://doi.org/10.1128/JB.186.24.8172-8180.2004.

34. Dorr T, Lewis K, Vulic M. 2009. SOS response induces persistence to fluoroquinolones in Escherichia coli. PLoS Genet 5:e1000760. https://doi.org/10.1371/journal.pgen.1000760.

35. Roghanian M, Semsey S, Løbner-Olesen A, Jalalvand F. 2019. (p)ppGpp-mediated stress response induced by defects in outer membrane biogenesis and ATP production promotes survival in Escherichia coli. Sci Rep 9:2934. https://doi.org/10.1038/s41598-019-39371-3.

36. Gerdes K, Maisonneuve E. 2015. Remarkable functional convergence: alarmone ppGpp mediates persistence by activating type I and II toxin-antitoxins. Mol Cell 59:1–3. https://doi.org/10.1016/j.molcel.2015.06.019.

37. Zhang Y, Zhang W, Liu S, Wu N, Zhang S, Yuan Y. 2017. Variable persister gene interactions with (p)ppGpp for persister formation in Escherichia coli. Front Microbiol 8:1795. https://doi.org/10.3389/fmicb.2017.01795.

38. Svenningsen MS, Veress A, Harms A, Mitarai N, Semsey S. 2019. Birth and resuscitation of (p)ppGpp induced antibiotic tolerant persister cells. Sci Rep 9:6056. https://doi.org/10.1038/s41598-019-42403-7.

39. Germain E, Castro-Roa D, Zenkin N, Gerdes K. 2013. Molecular mechanism of bacterial persistence by HipA. Mol Cell 52:248–254. https://doi.org/10.1016/j.molcel.2013.08.045.

40. Amato SM, Brynildsen MP. 2015. Persister heterogeneity arising from a single metabolic stress. Curr Biol 25:2090–2098. https://doi.org/10.1016/j.cub.2015.06.034.

41. Pu Y, Zhao Z, Li Y, Zou J, Ma Q, Zhao Y, Ke Y, Zhu Y, Chen H, Baker MAB, Ge H, Sun Y, Xie XS, Bai F. 2016. Enhanced efflux activity facilitates drug tolerance in dormant bacterial cells. Mol Cell 62:284–294. https://doi.org/10.1016/j.molcel.2016.03.035.

42. Hu Y, Kwan BW, Osbourne DO, Benedik MJ, Wood TK. 2015. Toxin YafQ increases persister cell formation by reducing indole signalling. Environ Microbiol 17:1275–1285. https://doi.org/10.1111/1462-2920.12567.

43. Kwan BW, Osbourne DO, Hu Y, Benedik MJ, Wood TK. 2015. Phosphodiesterase DosP increases persistence by reducing cAMP which reduces the signal indole. Biotechnol Bioeng 112:588–600. https://doi.org/10.1002/bit.25456.

44. Hirakawa H, Inazumi Y, Masaki T, Hirata T, Yamaguchi A. 2005. Indole induces the expression of multidrug exporter genes in Escherichia coli. Mol Microbiol 55:1113–1126. https://doi.org/10.1111/j.1365-2958.2004.04449.x.

45. Kobayashi A, Hirakawa H, Hirata T, Nishino K, Yamaguchi A. 2006. Growth phase-dependent expression of drug exporters in Escherichia coli and its contribution to drug tolerance. J Bacteriol 188:5693–5703. https://doi.org/10.1128/JB.00217-06.

46. Pu Y, Li Y, Jin X, Tian T, Ma Q, Zhao Z, Lin S, Chen Z, Li B, Yao G, Leake MC, Lo C-J, Bai F. 2018. ATP-dependent dynamic protein aggregation regulates bacterial dormancy depth critical for antibiotic tolerance. Mol Cell 73:143–156.e4. https://doi.org/10.1016/j.molcel.2018.10.022.

47. Slonczewski JL, Rosen BP, Alger JR, Macnab RM. 1981. pH homeostasis in Escherichia coli: measurement by 31P nuclear magnetic resonance of methylphosphonate and phosphate (pH regulation/intracellular pH/protonmotive force/Fourier-transform NMR). Proc Natl Acad Sci U S A 78:6271–6275. https://doi.org/10.1073/pnas.78.10.6271.

48. Padan E, Zilberstein D, Schuldiner S. 1981. pH homeostasis in bacteria. Biochim Biophys Acta 650:151–166. https://doi.org/10.1016/0304-4157(81)90004-6.

49. Krulwich TA, Sachs G, Padan E. 2011. Molecular aspects of bacterial pH sensing and homeostasis. Nat Rev Microbiol 9:330–343. https://doi.org/10.1038/nrmicro2549.

50. Padan E, Zilberstein D, Rottenberg H. 1976. The proton electrochemical gradient in Escherichia coli cells. Eur J Biochem 63:533–541. https://doi.org/10.1111/j.1432-1033.1976.tb10257.x.

51. Padan E, Venturi M, Gerchman Y, Dover N. 2001. Na+/H+ antiporters. Biochim Biophys Acta 1505:144–157. https://doi.org/10.1016/S0005-2728(00)00284-X.

52. Padan E, Bibi E, Ito M, Krulwich TA. 2005. Alkaline pH homeostasis in bacteria: new insights. Biochim Biophys Acta 1717:67–88. https://doi.org/10.1016/j.bbamem.2005.09.010.

53. Castanie-Cornet MP, Penfound TA, Smith D, Elliott JF, Foster JW. 1999. Control of acid resistance in Escherichia coli. J Bacteriol 181:3525–3535. https://doi.org/10.1128/JB.181.11.3525-3535.1999.

54. Schuldiner S, Agmon V, Brandsma J, Cohen A, Friedman E, Padan E. 1986. Induction of SOS functions by alkaline intracellular pH in Escherichia coli. J Bacteriol 168:936–939. https://doi.org/10.1128/jb.168.2.936-939.1986.

55. Taglicht D, Padan E, Oppenheim AB, Schuldiner S. 1987. An alkaline shift induces the heat shock response in Escherichia coli. J Bacteriol 169:885–887. https://doi.org/10.1128/jb.169.2.885-887.1987.

56. Zarkan A, Caño-Muñiz S, Zhu J, Al Nahas K, Cama J, Keyser UF, Summers DK. 2019. Indole pulse signalling regulates the cytoplasmic pH of E. coli in a memory-like manner. Sci Rep 9:3868. https://doi.org/10.1038/s41598-019-40560-3.

57. Gaimster H, Cama J, Hernández-Ainsa S, Keyser UF, Summers DK. 2014. The indole pulse: a new perspective on indole signalling in Escherichia coli. PLoS One 9:e93168. https://doi.org/10.1371/journal.pone.0093168.

58. Zarkan A, Liu J, Matuszewska M, Gaimster H, Summers DK. 2020. Local and universal action: the paradoxes of indole signalling in bacteria. Trends Microbiol 28:566–577. https://doi.org/10.1016/j.tim.2020.02.007.

59. Lee J, Jayaraman A, Wood TK. 2007. Indole is an inter-species biofilm signal mediated by SdiA. BMC Microbiol 7:42. https://doi.org/10.1186/1471-2180-7-42.

60. Lee J-H, Wood TK, Lee J. 2015. Roles of indole as an interspecies and interkingdom signaling molecule. Trends Microbiol 23:707–718. https://doi.org/10.1016/j.tim.2015.08.001.

61. Bansal T, Alaniz RC, Wood TK, Jayaraman A. 2010. The bacterial signal indole increases epithelial-cell tight-junction resistance and attenuates indicators of inflammation. Proc Natl Acad Sci U S A 107:228–233. https://doi.org/10.1073/pnas.0906112107.

62. Di Martino P, Fursy R, Bret L, Sundararaju B, Phillips RS. 2003. Indole can act as an extracellular signal to regulate biofilm formation of Escherichia coli and other indole-producing bacteria. Can J Microbiol 49:443–449. https://doi.org/10.1139/w03-056.

63. Bommarius B, Anyanful A, Izrayelit Y, Bhatt S, Cartwright E, Wang W, Swimm AI, Benian GM, Schroeder FC, Kalman D. 2013. A family of indoles regulate virulence and Shiga toxin production in pathogenic E. coli. PLoS One 8:e54456. https://doi.org/10.1371/journal.pone.0054456.

64. Lee HH, Molla MN, Cantor CR, Collins JJ. 2010. Bacterial charity work leads to population-wide resistance. Nature 467:82–86. https://doi.org/10.1038/nature09354.

65. Vega NM, Allison KR, Khalil AS, Collins JJ. 2012. Signaling-mediated bacterial persister formation. Nat Chem Biol 8:431–433. https://doi.org/10.1038/nchembio.915.

66. Kuczyńska-Wiśnik D, Stojowska K, Matuszewska E, Leszczyńska D, Moruno Algara M, Augustynowicz M, Laskowska E. 2015. Lack of intracellular trehalose affects formation of Escherichia coli persister cells. Microbiology (Reading) 161:786–796. https://doi.org/10.1099/mic.0.000012.

67. Wang Y, Tian T, Zhang J, Jin X, Yue H, Zhang X-H, Du L, Bai F. 2019. Indole reverses intrinsic antibiotic resistance by activating a novel dual-function importer. mBio 10:e00676-19. https://doi.org/10.1128/mBio.00676-19.

68. Kim JS, Yamasaki R, Song S, Zhang W, Wood TK. 2018. Single cell observations show persister cells wake based on ribosome content. Environ Microbiol 20:2085–2098. https://doi.org/10.1111/1462-2920.14093.

69. Song S, Wood TK. 2021. 'Viable but non-culturable cells' are dead. Environ Microbiol 23:2335–2338. https://doi.org/10.1111/1462-2920.15463.

70. Sankaranarayanan S, De Angelis D, Rothman JE, Ryan TA. 2000. The use of pHluorins for optical measurements of presynaptic activity. Biophys J 79:2199–2208. https://doi.org/10.1016/S0006-3495(00)76468-X.

71. Miesenböck G, De Angelis DA, Rothman JE. 1998. Visualizing secretion and synaptic transmission with pH-sensitive green fluorescent proteins. Nature 394:192–195. https://doi.org/10.1038/28190.

72. Albertazzi L, Arosio D, Marchetti L, Ricci F, Beltram F. 2009. Quantitative FRET analysis with the E0GFP-mCherry fluorescent protein pair. Photochem Photobiol 85:287–297. https://doi.org/10.1111/j.1751-1097.2008.00435.x.

73. Wang P, Robert L, Pelletier J, Dang WL, Taddei F, Wright A, Jun S. 2010. Robust growth of Escherichia coli. Curr Biol 20:1099–1103. https://doi.org/10.1016/j.cub.2010.04.045.

74. Stone MRL, Łapińska U, Pagliara S, Masi M, Blanchfield JT, Cooper MA, Blaskovich MAT. 2020. Fluorescent macrolide probes—synthesis and use in evaluation of bacterial resistance. RSC Chem Biol 1:395–404. https://doi.org/10.1039/D0CB00118J.

75. Cama J, Voliotis M, Metz J, Smith A, Iannucci J, Keyser UF, Tsaneva-Atanasova K, Pagliara S. 2020. Single-cell microfluidics facilitates the rapid quantification of antibiotic accumulation in Gram-negative bacteria. Lab Chip 20:2765–2775. https://doi.org/10.1039/d0lc00242a.

76. Smith A, Kaczmar A, Bamford RA, Smith C, Frustaci S, Kovacs-Simon A, O'Neill P, Moore K, Paszkiewicz K, Titball RW, Pagliara S. 2018. The culture environment influences both gene regulation and phenotypic heterogeneity in Escherichia coli. Front Microbiol 9:1739. https://doi.org/10.3389/fmicb.2018.01739.

77. Bartek IL, Reichlen MJ, Honaker RW, Leistikow RL, Clambey ET, Scobey MS, Hinds AB, Born SE, Covey CR, Schurr MJ, Lenaerts AJ, Voskuil MI. 2016. Antibiotic bactericidal activity is countered by maintaining pH homeostasis in Mycobacterium smegmatis. mSphere 1:e00176-16. https://doi.org/10.1128/mSphere.00176-16.

78. Casey JR, Grinstein S, Orlowski J. 2010. Sensors and regulators of intracellular pH. Nat Rev Mol Cell Biol 11:50–61. https://doi.org/10.1038/nrm2820.

79. Kim JS, Chowdhury N, Yamasaki R, Wood TK. 2018. Viable but non-culturable and persistence describe the same bacterial stress state. Environ Microbiol 20:2038–2048. https://doi.org/10.1111/1462-2920.14075.

80. Foster JW. 2004. Escherichia coli acid resistance: tales of an amateur acidophile. Nat Rev Microbiol 2:898–907. https://doi.org/10.1038/nrmicro1021.

81. Yohannes E, Barnhart DM, Slonczewski JL. 2004. pH-dependent catabolic protein expression during anaerobic growth of Escherichia coli K-12. J Bacteriol 186:192–199. https://doi.org/10.1128/JB.186.1.192-199.2004.

82. Gut H, Pennacchietti E, John RA, Bossa F, Capitani G, De Biase D, Grütter MG. 2006. Escherichia coli acid resistance: pH-sensing, activation by chloride and autoinhibition in GadB. EMBO J 25:2643–2651. https://doi.org/10.1038/sj.emboj.7601107.

83. Noguchi K, Riggins DP, Eldahan KC, Kitko RD, Slonczewski JL. 2010. Hydrogenase-3 contributes to anaerobic acid resistance of escherichia coli. PLoS One 5:e10132. https://doi.org/10.1371/journal.pone.0010132.

84. Scherzer R, Gdalevsky GY, Goldgur Y, Cohen-Luria R, Bittner S, Parola AH. 2009. New tryptophanase inhibitors: towards prevention of bacterial biofilm formation. J Enzyme Inhib Med Chem 24:350–355. https://doi.org/10.1080/14756360802187612.

85. Weber H, Polen T, Heuveling J, Wendisch VF, Hengge R. 2005. Genome-wide analysis of the general stress response network in Escherichia coli: σS-dependent genes, promoters, and sigma factor selectivity. J Bacteriol 187:1591–1603. https://doi.org/10.1128/JB.187.5.1591-1603.2005.

86. Bergholz TM, Wick LM, Qi W, Riordan JT, Ouellette LM, Whittam TS. 2007. Global transcriptional response of Escherichia coli O157:H7 to growth transitions in glucose minimal medium. BMC Microbiol 7:97–27. https://doi.org/10.1186/1471-2180-7-97.

87. Imdahl F, Vafadarnejad E, Homberger C, Saliba AE, Vogel J. 2020. Single-cell RNA-sequencing reports growth-condition-specific global transcriptomes of individual bacteria. Nat Microbiol 5:1202–1206. https://doi.org/10.1038/s41564-020-0774-1.

88. Thomson NM, Shirai T, Chiapello M, Kondo A, Mukherjee KJ, Sivaniah E, Numata K, Summers DK. 2018. Efficient 3-hydroxybutyrate production by quiescent Escherichia coli microbial cell factories is facilitated by indole-induced proteomic and metabolomic changes. Biotechnol J 13:e1700571. https://doi.org/10.1002/biot.201700571.

89. Zarkan A, Matuszewska M, Trigg SB, Zhang M, Belgami D, Croft C, Liu J, El-Ouisi S, Greenhalgh J, Duboff JS, Rahman T, Summers DK. 2020. Inhibition of indole production increases the activity of quinolone antibiotics against. Sci Rep 10:11742. https://doi.org/10.1038/s41598-020-68693-w.

90. Lee JH, Lee J. 2010. Indole as an intercellular signal in microbial communities. FEMS Microbiol Rev 34:426–444. https://doi.org/10.1111/j.1574-6976.2009.00204.x.

91. Datsenko KA, Wanner BL. 2000. One-step inactivation of chromosomal genes in Escherichia coli K-12 using PCR products. Proc Natl Acad Sci U S A 97:6640–6645. https://doi.org/10.1073/pnas.120163297.

92. Baba T, Ara T, Hasegawa M, Takai Y, Okumura Y, Baba M, Datsenko KA, Tomita M, Wanner BL, Mori H. 2006. Construction of Escherichia coli K-12 in-frame, single-gene knockout mutants: the Keio collection. Mol Syst Biol 2:2006.0008. https://doi.org/10.1038/msb4100050.

93. Kim J, Webb AM, Kershner JP, Blaskowski S, Copley SD. 2014. A versatile and highly efficient method for scarless genome editing in Escherichia coli and Salmonella enterica. BMC Biotechnol 14:84. https://doi.org/10.1186/1472-6750-14-84.

94. Gibson DG, Young L, Chuang RY, Venter JC, Hutchison CA, Smith HO. 2009. Enzymatic assembly of DNA molecules up to several hundred kilobases. Nat Methods 6:343–345. https://doi.org/10.1038/nmeth.1318.

95. Locatelli E, Pierno M, Baldovin F, Orlandini E, Tan Y, Pagliara S. 2016. Single-file escape of colloidal particles from microfluidic channels. Phys Rev Lett 117:e038001. https://doi.org/10.1103/PhysRevLett.117.038001.

96. Smith A, Metz J, Pagliara S. 2019. MMHelper: an automated framework for the analysis of microscopy images acquired with the mother machine. Sci Rep 9:10123. https://doi.org/10.1038/s41598-019-46567-0.

97. Love MI, Huber W, Anders S. 2014. Moderated estimation of fold change and dispersion for RNA-seq data with DESeq2. Genome Biol 15:550. https://doi.org/10.1186/s13059-014-0550-8.

98. Scrucca L, Fop M, Murphy TB, Raftery AE. 2016. mclust 5: clustering, classification and density estimation using Gaussian finite mixture models. R J 8:289–317. https://doi.org/10.32614/RJ-2016-021.

99. Yu G, Wang LG, Han Y, He QY. 2012. clusterProfiler: an R package for comparing biological themes among gene clusters. OMICS 16:284–287. https://doi.org/10.1089/omi.2011.0118.

100. Benjamini Y, Hochberg Y. 1995. Controlling the false discovery rate: a practical and powerful approach to multiple testing. J R Stat Soc B 57:289–300. https://doi.org/10.1111/j.2517-6161.1995.tb02031.x.

101. Liu J, Summers D. 2017. Indole at low concentration helps exponentially growing Escherichia coli survive at high temperature. PLoS One 12:e018853. https://doi.org/10.1371/journal.pone.0188853.